Article

Modeling the Dynamic Concentration Profiles and Efficacy of Type-I and Type-II Photopolymerization

Jui-Teng Lin [1], Da-Chuan Cheng [2], Kuo-Ti Chen [3], and Hsia-Wei Liu [4,*]

[1] New Vision Inc., 10F, No. 55, Sect.3, Xinbei Blvd, Xinzhung, New Taipei City, Taiwan; jtlin55@gmail.com
[2] Department of Biomedical Imaging and Radiological Science, China Medical University, Taichung 404, Taiwan; dccheng@mail.cmu.edu.tw
[3] Graduate Institute of Applied Science and Engineering, Fu Jen Catholic University, New Taipei City, Taiwan; tony022199@msn.com
[4] Department of Life Science, Fu Jen Catholic University, New Taipei City, Taiwan; 079336@gmail.com

* Author to whom correspondence should be addressed; Hsia-Wei Liu, e-Mail: 079336@gmail.com

ABSTRACT: The kinetics and efficacy profiles of photoinitiated polymerization are theoretically presented. For the same dose, lower light intensity achieves a higher steady-state-efficacy (SSE) in type-I; in contrast, type-II has an equal SSE. Higher light intensity has a faster rising efficacy, due to faster depletion of photoinitiator (PS) concentration. However, type-II process is also affected by the available oxygen. Higher light intensity produces more efficient singlet oxygen, resulting a higher transient efficacy, in which all intensities reach the same SSE when oxygen is completely depleted. With external oxygen, type-II efficacy increases with time, otherwise, it is governed only by the light dose, i.e., same dose achieves same efficacy. Moreover, type-II has an efficacy follows Bunsen Roscoe law (BRL), whereas type-I follows non-BRL. The measured type-I efficacy and gelation profile are analyzed by our analytic formulas. Schematics of the photocrosslinking stage defined by the availability of oxygen is developed, where both type-I and –II coexist until the oxygen is depleted. The overall efficacy may be enhanced by resupply of PS or oxygen during the light exposure. The roles of light dose and PS concentration on the efficacy of photoinitiated polymerization should be are governed a new concept of a volume efficacy (Ve), defined by the product of the crosslink (or gelation) depth (CD) and local [efficacy].

Keywords: polymerization; modeling; kinetic; singlet oxygen; polymerization efficacy; crosslinking

1. Introduction

External stimuli such as such as pH, temperature, hydrophobicity, the presence of ions or enzymes, and light-stimulation will cause the three-dimensional polymeric networks, called hydrogels, to be physically or chemically linked for "gelation", or crosslinking [1,2]. These processes result in the increasing of polymer networks and viscosity of the medium, but decreasing solubility of polymers. Physically-assembled gels are built with polymer networks tied via hydrogen bonds, ionic interactions, hydrophobic associations, or agglomerations. Chemically-linked hydrogels are commonly prepared via a three-dimensional polymerization using a water-soluble monomeric polymer and a multi-functional cross-linker [2]. Photoinitiated polymerization and crosslinking provide advantageous means over the thermal-initiated polymerization, including fast and controllable reaction rates, spatial and temporal control over the formation of the material, and without a need for high temperatures or pH conditions [1,2].

Photodynamic therapy (PDT) offers biometrical applications in dermatology, orthopedics (tissue engineering), ophthalmology and cancer treatments in various parts of human body, including early stage (micro-invasive) lung cancer, lung tumors (endobronchial, mesothelioma), skin,

 doi:10.20944/preprints201805.0472.v2

brain, colorectal and breast cancer, chronic skin diseases (psoriasis, vitiligo), and oral cavity (anti-bacterial, curing) [7-14]. Ophthalmology applications include age-related macular degeneration (AMD), coagulation of retina and corneal crosslinking for keratoconus and ulcers [15-17].

The kinetics of photoinitiated polymerization systems (PPS) have been studied by many researchers for uniform photoinitiator distribution or for the over simplified cases that the photolysis product becomes completely transparent after polymerization or constant light intensity [18-23]. Kinetic modeling of PPS assumed either a constant light intensity (for thin polymers), or a conventional Beer-Lambda law for the light intensity [13, 18-20]. For more realistic systems, the distribution of the photoinitiator is non-uniform and the UV light may still be absorbed by the photolysis product besides the absorption of the monomer. To improve the efficiency and spatial uniformity (in the depth direction) particularly in a thick system (>1.0 cm), we have presented the numerical results using a focused light [24] and two-beam approach [25] for the case of uniform PS distribution; and analytic and computer modeling for the non-uniform case [26]. Optimal efficacy in light-activated biomedical systems and nonlinear laws versus linear Beer-Lambert law were also reported by Lin [27].

The kinetics and macroscopic modeling of PPS for anti-cancer have been reported by Zhu et al [13] and Kim et al [14], which, however, are limited to the type-II oxygen-mediated process. Lin reported the kinetic modeling for both type-I and type-II mechanism for the application in corneal collagen crosslinking (CXL) [16,17,28], where the temporal and spatial profiles of PS concentration and the CXL efficacy were also reported. Accelerated CXL has been clinically used for faster procedure (within 3 to 10 minutes) using higher light intensity of 9 to 45 mW/cm^2, in replacing the conventional 3 mW/cm^2 which took 30 minutes [29]. However, much less efforts have been done for fast PPS in thick polymers using a high light intensity.

Photo-polymerization offers two major categories of biomedical applications: (a) photodynamic therapy (PDT) using light-initiated oxygen free radical; and (b) crosslinking (or gelation) of biomaterials using radical-substrate coupling for tissue engineering [1,2]. In general, both type-I and type-II reactions can occur simultaneously, and the ratio between these processes depends on the types and the concentrations of PS, substrate and oxygen, the kinetic rates involved in the process [16,17]. Kim et al [14] have focused on the type-II oxygen-mediated process, whereas we have previously focused on the non-oxygen-mediated type-I mechanism [27]. It is not yet fully understood, theoretically or experimentally, the interaction between these two mechanisms.

In this study, we will further study the oxygen-mediated type-II mechanism, and compare the significant different kinetics and efficacy of type-I and type-II by numerical simulations and analytic formulas. Dynamic profiles of singlet-oxygen concentration, polymerization efficacy, and the cell viability are produced by numerical solutions of macroscopic equations. Depending on the rate constant, type-I and type-II mechanism may coexist to achieve a higher efficacy than type-II dominant case, which is limited by the available oxygen. We will also explore the new strategy to enhance the overall efficacy by resupply of PI or oxygen during the light exposure.

2.Methods and Modeling systems

2.1. Photochemical kinetics

The kinetics of corneal collagen crosslinking (CXL) shown by Fig. S-1 (shown in Supporting Information) was previously reviewed by Lin [17] using UVA (365 nm) initiated riboflavin solution as the sensitizer. Fig. 1 shows the 4 coupled dynamic equations defined as dI/dz, d[C]/dt, d[T]/dt and d[O_2]/dt, for, respectively, light intensity, PS concentration, triplet state, and oxygen molecular. The three pathways are revised for a more general polymer system as shown in Fig. 1 and briefly summarized as follows. In type-I pathway, the excited PS triple-state (T_3) can interact directly with the substrate (A); or with the ground state oxygen (O_2) to generate a superoxide anion (O^-), which further reacts with oxygen to produce reactive oxygen species (ROS). In comparison, in type-II pathway, T_3 interacts with (O_2) to form a reactive singlet oxygen (O*). In general, both type-I and type-II reactions can occur simultaneously, and the ratio between these processes depends on the

Preprints (www.preprints.org) | NOT PEER-REVIEWED | Posted: 30 October 2018 doi:10.20944/preprints201805.0472.v2

types and the concentrations of PS, substrate and oxygen, the kinetic rates involved in the process [16].

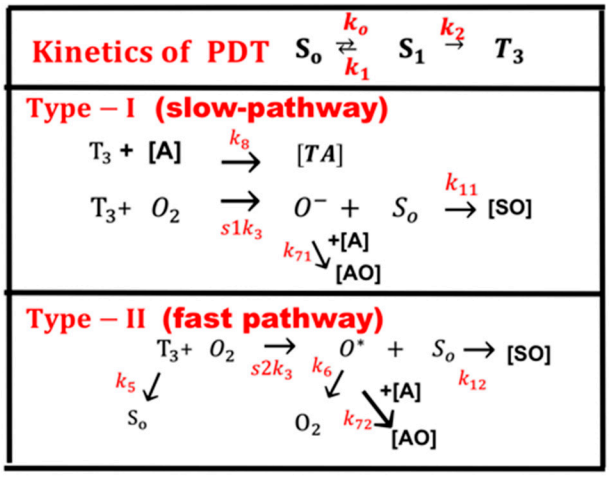

Fig. 1 The kinetics of PDT, where [S_0], [S_1] and [T_3] are the ground state, singlet excited state, and triplet excited state of PS molecules. Three pathways are shown for both type-I and type-II process. Ground state oxygen may couple to T_3 to form either singlet oxygen [O*], or other reactive radicals [O-]. In type-I pathway, T_3 can interact directly with the collagen substrate (A); or with the oxygen (O_2) to generate a superoxide anion (O^-); in type-II pathway, T_3 interacts with the ground oxygen (O_2) to form a singlet oxygen (O*) [16].

These factors also influence the overall photopolymerization efficacy, particularly the PS triplet state quantum yield (q) and its concentration. Furthermore, the specific protocols and the methods of PS instillations prior to and during the photopolymerization also affect the short and long term outcomes. The overall photopolymerization efficacy is proportional to the time integration of the light intensity, I (z, t) and the PS and oxygen concentration, C (z, t), and [O_2]. The efficacy reaches a saturated (steady) state when C (z, t) or [O_2] is depleted by the light, where higher intensity depletes C (z, t) and [O_2] faster and therefore reaches a lower steady-state efficacy [26,29].

Referring to the kinetic pathways shown by Fig. 1, a set of quasi steady-state macroscopic kinetic equation for the PI ground-state, C (z, t), and the ground state oxygen molecule [O_2] is constructed [14,16]

$$\frac{\partial C(z,t)}{\partial t} = -b[g + g']C \tag{1.a}$$

$$\frac{\partial [O_2]}{\partial t} = -sbCG + P \tag{1.b}$$

$$\frac{\partial I(z,t)}{\partial z} = -A'(z,t)I(z,t) \tag{1.c}$$

$$A'(z,t) = 2.3[(a' - b')C(z,t) + b'C_0(z) + Q] \tag{1.d}$$

where b=aqI (z, t); a=83.6wa'; w is the light wavelength; a' and b' are the molar extinction coefficient of the initiator and the photolysis product, respectively; Q is the absorption coefficient of the monomer and the polymer repeat unit. Typical values are [4,9]: a'=0.2 to 0.3 (1/mM/cm), b'=0.1 to 0.15 (1/mM/cm)), and C_0= 1.0 to 3.0 mM; and for a UV light at 365 nm, a=0.00305a' (1/cm).

For type-I, g=k_8[A]G_0/k_3, G_0=1/([O_2] +k+K'); and for type-II, g'=K'(C+d) G(z), with G(z)= [O_2] G_0, k=(k_5+k_8[A])/k_3; K'= k_{12}/ (k_6+ k_{12}(C+d) + k_{72}[A]); d is a low concentration correction related to the diffusion of singlet oxygen [14]. [A] is the substrate concentration. q is the triplet state [T] quantum yield given by q=k_2/(k_1+k_2); s=s1+s2, with s_1 and s_2 are the fraction of [O_2] converted to the singlet

Preprints (www.preprints.org) | NOT PEER-REVIEWED | Posted: 30 October 2018 doi:10.20944/preprints201805.0472.v2

oxygen and other ROS, respectively, in type-I and type-II [16]. All other rate constants, kj, k_{ij} are defined by the reaction paths shown in Fig. 1.

In Eq. (1.b) we have included the light intensity in the polymer given by a time-dependent Beer-Lambert law [27]. We have also included in Eq. (1.b) the oxygen source term P (z, t) =p(1-[O2]/[O_0]), with a rate constant p to count for the situation when there is an external continuing supply, or nature replenishment (at a rate of p), besides the initial oxygen, [O_0], in the polymer.

We note that Eq. (1) was also presented by Kim et al [14] for the anti-cancer kinetics. However, they have assumed a constant UV intensity, i.e., A′ (z, t) is a constant in Eq. (1.d). They also ignored the contribution from the type-I term, k_8[A], since type-II is dominant in their anti-cancer process. Most of the previous model have also ignored the dynamic of UV intensity given by Eq. (1.c) and the depth-dependent profile of PI and light intensity [18-20]. Exact solutions of Eq. (1) require numerical simulations. For analytic formulas, we will use an effective A (z, t) or its mean value, such that A′ (z, t) becomes time-independent in solving Eq. (1). The effective absorption is given by [28], The effective absorption is given by [28], A′=2.3x0.5(a'+b') (1-0.25z/D) C_0+Q.

2.2. *Concentration Profile, Crosslink (or gelation) Time and Depth*

In solving Eq. (1), we will choose initial profile (at t=0) I_0(z)=I_0(1-0.25z/D) for the light intensity; and C_0(z)=C_0F(z), with F(z)=1-0.5z/D, for the PS concentration distribution; where D is the PS concentration distribution depth; and when D>> 1.0 cm, F=1 representing a flat (or uniform) PS distribution. Analytic solution of Eq. (1) is available for the type-I process and under certain approximation. For g>>g′, or for the case that type-I is dominant over type-II, we obtain an approximate solution, C (z, t) = C_0F(z)exp(-bgt), assuming b and g are time-independent, or taking their averaged value. A′ (z, t) in Eq. (1.d) has an initial value (A_1, with b'=0) and steady state value (A_2, with C=0), given by: A_1=2.3[a′C_0F′+Q], and A_2=2.3[b′C_0F′+Q], with F′(z)=1-0.25z/D being the integration of F(z) over z; the mean value is given by A=0.5(A_1+A_2). We have also developed numerically fit value [9], A=2.3[mb′C_0F + Q], with m=0.8 to 1.0 depending on the value of a′ and b′.

A crosslink (or gelation) time T* may be defined by when the PS concentration C (z, t=T*) =C_0(z)exp(-M), with M = 4, or C (z, t) is depleted to 0.018 of its initial value. We obtain an analytic formula T*(z)=T_0 exp(Az), where T_0 is the surface depletion time given by T_0=M/(bg), which is inverse proportional to the light initial intensity, since b=aqI(z). T* may be also defined by the level of photopolymerization efficacy, or the crosslink time (Tc), to be discussed later. The strong depletion of C (z, t) will also affect the time-dependent profiles of the intensity, I (z, t), which in general, will not follow the conventional Beer-Lambert law (BLL), and should be governed by a generalized, time-dependent BLL first presented by Lin [27,28].

Another important parameter is called crosslink (or gelation) depth (z*) may be defined by the depth having PS concentration C (z*, t=T*) reduced to a low value of C′ which typically is (1/e^4, or 0.18%) of its initial value (at t=T*). Therefore, it is given by (for the case of flat distribution or F=1) z*=(1/A)ln(bE_0/M), with M=ln (C_0/C′), which is proportional to the light fluence (or dose), E_0. In general, for F<1 (with D< 1.0 cm) and A is z-dependent, z* needs numerical calculation.

2.3. *Efficacy Profiles*

The normalized photo-polymerization efficacy defined by Ceff =1-[A]/[A]$_0$ = 1-exp(-S), with S-function for type-I (S_1) and type-II (S_2), and the overall efficacy is given by Ceff=1-exp[-(S_1+S_2)]. The type-I efficacy may be further expressed by rate equation of conversion of collagen monomers [M] to polymers, where the NOM term of Eq. (1.a), g=k_8[A]G_0/k_3, is replaced by an overall rate constant (K) including all polymerization chain reactions. The S functions are given by [13,16]

$$S_1 = \int_0^t [\sqrt{aqgK\,IC} + (fs_1 aqK')I(z,t)G]\,dt \qquad (3.a)$$

for type-I, and

Preprints (www.preprints.org) | NOT PEER-REVIEWED | Posted: 30 October 2018 doi:10.20944/preprints201805.0472.v2

$$S_2 = \int_0^t f s_2 aq K' I(z,t) G \, dt \quad (2.b)$$

for type-II.

The first term in Eq. (3.a) relates to the direct coupling of triplet state [T] with the substrate [A] under hypoxic conditions or any other non-oxygen-mediated (NOM) reactions; and the second term relates with the reactive oxygen species (ROS)-mediated reactions (in type-I). f is the fraction of all ROS (including singlet oxygen) interacting with acceptors [A], or the oxygen-mediated (OM) reactions in type-I and type-II. s_2 and s_1 are the fraction of $[O_2]$ interacting with [T] to produce singlet oxygen (in type-II) and other ROS (in type-I), respectively.

2.4. Analytic formulas

For analytic formulas, we will use the mean value of A(z) such that $I(z, t) = I_0 \exp(-Az)$, and $C(z, t) = C_0 F \exp(-Bt)$, with $B = bg = aqgI(z)$, Eq. (3.a), for the case that $g' \ll g$, the type-I, S- function is given by [16,28]

$$S_1 = \sqrt{4KCoF \exp(Az)/(aqgIo)}\; E1 \quad (4.a)$$

$$E1 = [1 - \exp(-0.5Bt)] \quad (3.b)$$

which is a nonlinear function of the light dose (E) given by its Taylor expansion $S_1 = \sqrt{(aqIoKCoF)}\exp(-Az)\, t[1 - 0.5aqgE + \cdots]$, which follows Bunsen–Roscoe reciprocal law (BRL) only for small time with the first term kept. In contrast, type-II efficacy, given by the time integral of [IC] follows the BRL [26]. A crosslink time (T) may be defined by Eq. (4.b) when E1=0.87, or 0.5BTc=2, which gives us $Tc = 4/B = 4/(bg) = [4/(aqgI_0)] \exp(Az) = T_0 \exp(Az)$, with the surface crosslink time given by $T_0 = 4/(aqgI_0) = 1000/I_0$, for aqg=0.004. We note that the crosslink time equals to the depletion time (T*), when M=4, and it also defines the gelation time, or crossover time.

Type-II process is much more complex than type-I and requires numerical solutions to be shown later. For analytic results for type-II dominant case (with $g' \gg g$), we assume an approximated oxygen concentration given by $[O_2] = [O_0] - m'btC_0$, with m' being a fit parameter; and the similar functional forms for C(z,t) and I(z,t) as type-I, the time integral of Eq. (3.b) gives us, for $k \ll [O_0]$ and P=0,

$$S_2 = (fsag)I'(z)C_0[(1 - k/[O_0])(E1 + dt) - HO \quad (5)$$

with $I'(z) = 0.5(I_1 + I_2) = 0.5I_0 \exp(-A'z)$, is a mean light intensity, and HO is a high-order term. Eq. (5) shows that the type-II efficacy is an increasing function of $I_0Co[O_0]$; and S_2 has a transient state (with E1= t) proportional to the light dose, I_0t; and steady-state is only dose-dependent (for the case of P=0) to be justified numerically later.

2.5. Nonlinear scaling law

As predicted by our S1 formula, the efficacy at transient state (for small dose) is proportional to $tI_0^{0.5}$, however, at steady-state, it is a nonlinear increasing function of $[C_0/I_0]^{0.5}$ or $[t/E_0]^{0.5}$. This nonlinear scaling law predicts the clinical data more accurate than the linear theory of Bunsen Roscoe law (BRL) [26]. Accelerated PPS based on BRL, therefore, has undervalued the exposure time (t) for higher intensity using the linear scaling of $t = [E_0/I_0]$, rather than $t = [E_0/I_0]^{0.5}$, based on our nonlinear law. To achieve the same efficacy, higher PS concentration requires higher light intensity; and for the same dose, higher light intensity requires a longer exposure time.

The BRL is based on the conventional Beer-Lambert law for light intensity without PS depletion, such that I(z) is time-independent, and C(z,t)=constant=C_0F, therefore, $S_1 = \sqrt{4KCoFEo \exp(Az)}$ which is a linear function of the dose $E_0 = (tI)$.

Our nonlinear law, as shown by Eq. (4) predicts that, for the same dose, higher intensity depletes the PS concentration faster and reach a lower steady-state efficacy. Further discussion will be shown later. As shown by our S-formula, diffusion depth (D) also pays important role. Larger D will achieve

 doi:10.20944/preprints201805.0472.v2

higher efficacy as shown by the PS distribution function, F(z)=1-0.5z/D, which is an increasing function of D, and F=1.0 for the flat (uniform) distribution case. The above features have been clinically shown in corneal crosslinking [26], but not yet for other PPS.

2.6. Volume efficacy

The new concept of a volume efficacy (Ve), first introduced by Lin [30], is defined by the product of the crosslink (or gelation) depth (CD) and local [efficacy], or Ve=z[1-exp(-S)], where z is the polymerization (or crosslink) depth (PD) given by z=(1/A)ln(b'/E_0), with b'=b/M, and E_0 is the light dose. For a type-II process, the local (at a specific depth z) efficacy is defined by Eff-=1-exp(-S), with S function is given by Eq. (3). For a polymer thickness of z_0, the normalized Ve is given by V'=Ve/z_0. For type-II application of anti-cancer for a cell sample thickness of z_0, the cell viability (normalized by z_0) is given by CV=1-Ve/z_0. We should note that both CD and S are increasing function of the light dose, however, they are competing functions with respective to the PS concentration. Higher C_0 offers higher S (or local efficacy) but it has a smaller depth (due to the larger absorption, or larger A-value). The general feature of Ve may be stated as follows: increasing light dose (for a fixed C_0) offers both higher [local efficacy] and [depth], and Ve; however, increasing C_0 (for a fixed light dose) suffers a shallow depth, although the [local efficacy] increases. Therefore, there is an optimal C_0 for maximum Ve. Numerical results and application for cell viability in anti-cancer and corneal crosslinking will be presented elsewhere.

3.Results and Discussions

3.1. Concentration profiles

Numerical results of Eq. (1) are shown in Fig. 3 for the PS concentration dynamic profiles, for a type-I dominant case, with g'<<g in Eq. (1.a). One may see that depletion of PS starts from the polymer surface, and gradually into the volume (z>0). We note that the PS concentration profile is an increasing function of z for the uniform case. In contrast, the non-uniform case shows a decreasing function of z.

3.2. Efficacy profiles

Using typical values of: a'=0.2(1/mM/cm), b'=0.1(1/mM/cm), Q=0.1 (1/cm), q=0.5, aqg=0.012 cm²/mW; the mean A(z)=0.35C_0F(z)+0.23, B=(0.006I_0) exp(-Az)., with C_0 in mM, I_0 in mW/cm². Eq. (4) gives a normalized S-function defined by S=S_1/S_0, where S_0=[4K/(aqg)]$^{0.5}$ is a proportional constant, such that $S = E1\sqrt{(CoF/Io)}\exp(Az)$.
In the follow figures, we will show the normalized S-function for S_0=4, or K/(aqg)=4. In addition, the transient factor E1 is based on aqg=0.012, or B=(aqg)I(z)=0.012I(z), and K=4(aqg)=0.048.

Fig. 2 compares the efficacy S-function profiles for: (A) type-I, and (B) type-II, for various light intensity, I_0 = (9,18,30,45) mW/cm², for curves (1,2,3,4). The important features demonstrated by Fig. 4 and 5 are summarized as follows:

(i) For the same dose, lower light intensity achieves a higher steady-state-efficacy (SSE) in type-I, as also shown by Eq. (4); in contrast to type-II, which has an equal SSE, as also shown by Eq. (5).

(ii) In both type-I and type-II, higher light intensity has a faster rising efficacy, due to faster depletion of PS concentration. However, type-II process is also affected by the available oxygen. Higher light intensity produces more efficient singlet oxygen, resulting a higher transient efficacy, as shown by Fig. 4-(B), in which all intensities reach the same SSE when oxygen is completely depleted, as shown by Fig. 4-(B).

(iii) As shown by Fig. S-2 (shown in Supporting Information), for the same dose, lower light intensity always achieves higher efficacy in type-I; in contrast, type-II efficacy is governed

Preprints (www.preprints.org) | NOT PEER-REVIEWED | Posted: 30 October 2018 doi:10.20944/preprints201805.0472.v2

only by the light dose (for the case of no external oxygen); i.e., same dose achieves same efficacy. Moreover, type-II has an efficacy follows BRL, whereas type-I follows non-BRL [27,17]. These numerical results are also predicted by our analytic formulas, Eq. (4) and (5).

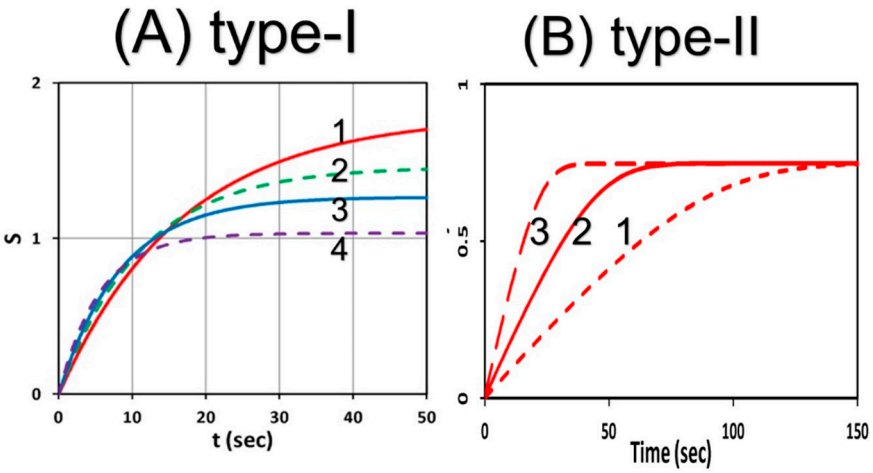

Fig. 2 Comparing the efficacy S-function temporal profiles for: (A) type-I, and (B) type-II, for various light intensity, I_0 = (9,18,30,45) mW/cm^2, for curves (1,2,3,4).

As shown by S-formulas, Eq. (5), for the anti-cancer type-II PDT efficacy S~ $[O_2]C$, which requires both PS concentration C and $[O_2]$. Therefore, resupply of PS or oxygen would enhance the generation of singlet oxygen radicals, and improve the anti-cancer efficacy via type-II PDT. Resupply of PS or oxygen during the light exposure would enhance the overall efficacy; this new strategy has been proposed in type-I corneal crosslinking [13], but not yet in gelation of thick polymers. These theoretically predicted features have been only partially proven clinically for corneal crosslinking [27]. Therefore, further experimental studies are highly desired in polymer systems.

3.3. Analysis of experiments

Our formula, Eq. (4), predicts that the type-I steady-state-S is proportional to the square-root of the PS concentration (C_0). Therefore, the crosslink efficacy, defined by Eff=1-exp(-S), is also an increasing function of C_0. This feature has been clinically reported by O'Brart et al in corneal crosslinking [30], where the PS is riboflavin solution initiated by a UVA light at 365 nm. The role of PS concentration was also shown by Table 1 of Holmes et al [31], where (for LAP) increasing the PS concentration from 0.1% to 0.5% (w/v) in the thiol-ene mixture resulted in a 15-fold increase in the storage modulus. This increasing feature may be analyzed by our S-function, Eq. (4), given by a steady-state formula $S'=S_0 [C_0 \exp(Az)]^{0.5}$. For C_0 increase five times, and for Az=0.9, we calculate S-function increases a factor of 2.23x exp(2Az) =14.5, which is comparable to the increase of storage modulus; noting that when C_0 is 5 times, A is also 5 times, given by $A=2.3mb'C_0F(z) + Q$, if $Q<<0.1$ (1/cm).

Fig. 3 of Holems et la [31] shows the gelation kinetic profiles which has a strong similarity as our Fig. 2 (red curve). The storage modulus was found to increase with time and UV exposure until a plateau was reached within 300 s, indicating no further elastic properties (complete chemical gel). The plateau-time corresponds to our crosslink time (T*) defined before. Similarly, the measured data of Shih et al [11] (in their Fig. 1) showed crosslinking of thiol-norbornene PEG- peptide hydrogels (initiated by a visible light). Also has a strong similarity as our Fig. 2 (red curve), except the time scale which depends on the types of PS and light used in the process. Unfortunately, Shih et al [11] and Holems et al [31] did not measure the profiles for different light intensity, as shown in our Fig. 2, to justify our predicted feature that higher light intensity is less efficient in gelation. However, our predicted feature has been clinically demonstrated in ophthalmic system for CXL [27].

Preprints (www.preprints.org) | NOT PEER-REVIEWED | Posted: 30 October 2018 doi:10.20944/preprints201805.0472.v2

Anti-cancer via oxygen-mediated type-II mechanism has been clinically studied [32,33], where the cytotoxic effect of photodynamic therapy (PDT) to tumor tissue is resulted by the generation of singlet oxygen. Efficacy of PDT is mainly influenced by: the concentration of PS drug accumulated into the cells, molecular oxygen in tissue, the light dose, intensity and dose (fluence) [34]. High concentrations of singlet oxygen can lead to necrotic cell death. In contrast, low concentrations lead to cell survival and increase the metabolism; whereas medium singlet oxygen concentrations lead to initiation of apoptosis or autophagy [32]. Therefore, the threshold light dose and singlet oxygen dose play the important role in PDT for anti-cancer. The singlet oxygen threshold dose, and the dose-dependence cell viability curves of human cancer cells of K562 and Hela after red-light irradiation of Radachlorin were reported in vivo by Klimenko et al [32]. They showed that the cell viability, defined by CV=exp(-S), is lower for higher C_0 and/or light intensity (I_0). Moreover, with p>o, external oxygen offers lower CV, or better cell killing. The threshold dose $E^*=I_0t^*$ (or time t* for a fixed light intensity) to reach a cell viability CV*<25%, is higher for smaller C_0 and/or I_0. These features are in consistent with our numerical results for type-II PDT to be shown later.

Above examples demonstrate that our formulas predict very well the measured results, at last the overall trends. However, the accuracy of our formulas will require accurate measurement of the parameters involved, such as the rate constant (K), the quantum yield (q), the molar extinction coefficient of the initiator (a'), the photolysis product (b'), and the monomer and the polymer repeat unit (Q) et al. In addition, further experimental measurements should also include the roles of PS concentration and light intensity. Our group has also worked on the in vitro measurement of cell viability, which may be empirically analyzed by our formulas, and results will be published elsewhere.

3.4. The role of oxygen

By solving the kinetic coupled Eq. (1) for oxygen, we have previously developed a schematic for type-I and type-II mechanisms in CXL, which has a very short oxygen depletion time (t*) approximately 10 to 30 seconds [16,17]. For thick polymer system, t* has a wide range of 50 to 500 seconds, depending on the PI, light intensity and kinetic rate constants. For example, in anti-cancer process, t* is few minutes and type-II process is predominant [14], whereas in CXL (with t*< 20 seconds), type-I is predominant. Therefore, we re-plot a schematic shown in Fig. 3 for a more general PPS without specifying t*. In the transient stage (with t<t*), both type-I and –II coexist until the oxygen is completely depleted; then type-I dominates before the oxygen is resupplied or replenished. In general, both type-I and type-II reactions can occur simultaneously, and the ratio between these processes depends on the types and the concentrations of PS, substrate and oxygen, and the kinetic rates involved in the process [17].

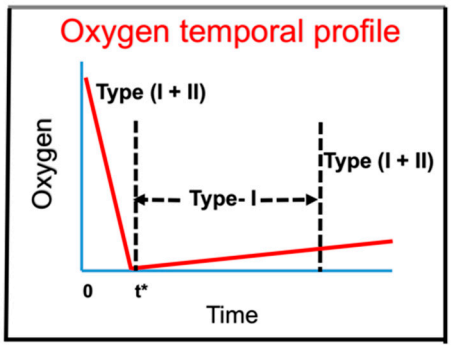

Fig. 3 Schematics of the oxygen profiles during the photocrosslinking process; in the transient stage, both type-I and –II coexist until the oxygen is depleted. (Figure revised from previous schematics [17]).

Preprints (www.preprints.org) | NOT PEER-REVIEWED | Posted: 30 October 2018 doi:10.20944/preprints201805.0472.v2

3.5. Numerical results

We will now explore the roles of each of the parameters involved in type-I and type-II mechanisms, where the macroscopic coupled Eq. (1) will be numerically solved for various parameters of: initial values, C_0, I_0, $[O_0]$, [A]; rate constants $k'=k_8/k_3$, $k=(k_5+k_8[A])/k_3$, K', small signal *d*, and the oxygen source term (p). The S functions defined by Eq. (2) will then calculated to obtain the associate singlet-oxygen concentration, efficacy, Eff=1-exp(-S), and the cell viability, CV=exp[-(S_1+S_2)]. Typical values are used in our calculations [13,14]: fixed $[O_0]$ =7.3(uM), k=11.9(uM), *d*= 33 (uM); and others will have ranges to show their roles: I_0= (50,100,200) mW/cm^2, C_0= (6,8.5,10) uM, [A]= (50,100) uM, k'= (0.0001, 0.05) 1/s. Above various parameters allow us to investigate the roles of [A], I_0, C_0, the interaction of type-I and type-II (via k') and the oxygen source term (p).

Fig. 4 shows the calculated temporal profiles of: (A) oxygen (red curves) and PS concentration (blue curves), (B) S_2-function, (C) cell viability, (D) efficacy vs. time, (E) singlet-oxygen, and (F) efficacy vs. light dose (E_0) for a small [A]=50 uM and k' value (0.0001), or type-II is dominant, whereas Fig. S-3 (in Supporting Information) shows the profiles for a higher [A]=100 uM which leads to a lower efficacy. Fig. S-4 (in Supporting Information) shows profiles with external oxygen supply, or P>0, where the type-II efficacy increases due to the resupply of oxygen, comparing Fig. (D) of Fig.4 and Fig.S-4. The role of substrate [A] is shown by Fig. S-5 (in Supporting Information) that higher [A]=100 uM has a lower type-II efficacy, but higher type-I efficacy. Fig. S-6 (in Supporting Information) shows the comparison of type-II S-profiles for the case without (*p*=0), and with external oxygen (*p*>0). We note that the efficacy is governed by the light dose only when p=0 and independent to light intensity; in contrast to *p*>0, which also shows the intensity-dependence for the transient state.

In contrast to Fig. 4 with a small k'=0.0001 (for type-II dominant), Fig. 5 shows profiles for a higher k'=0.05, in which type-I and type-II coexist. Comparing to Fig. 4(A), Fig. 5(A) shows more depletion of PS concentration, C (z, t), due to the combined type-I and type-II, which also shows higher efficacy and lower cell viability, as shown by Fig. (C) and (D). We note that, as shown by Fig. 5 (B) and (F), S_2 reaches its steady state, when oxygen is completely depleted; in contrast, S_1, is an increasing function of PS concentration and does not require oxygen.

The singlet oxygen threshold dose, and the dose-dependence cell viability curves after red-light irradiation of Radachlorin were reported in vivo by Klimenko et al [32], in which their Fig. 5 may be compared with our Fig. (C) of Fig. S-4 (in Supporting Information). Our group has also worked on the in vitro measurement of cell viability, which may be empirically analyzed by our numerical data (results will be published elsewhere). Resupply of PS or oxygen during the light exposure would enhance the overall efficacy. This new strategy has been proposed in type-I corneal crosslinking by Lin [29] and type-II anti-cancer by Lin et al [35].

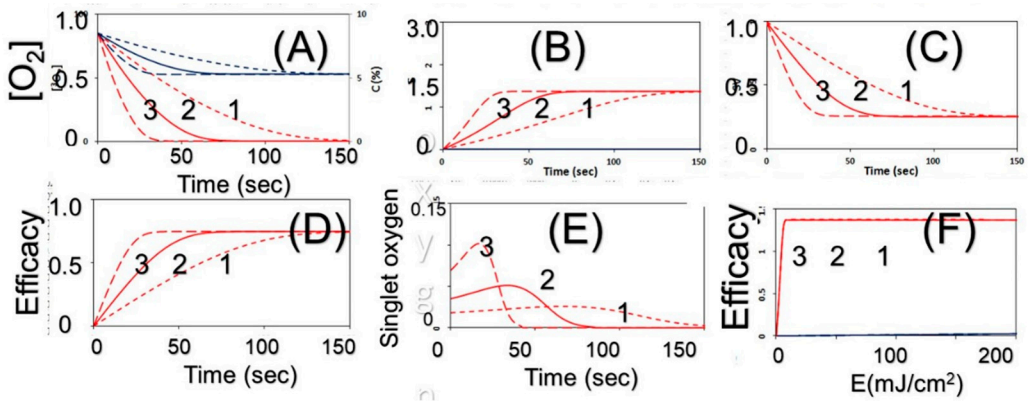

Fig. 4 The calculated temporal profiles of: (A) oxygen (red curves) and PS concentration (blue curves), (B) S_2-function, (C) cell viability, (D) efficacy vs. time, (E) singlet-oxygen, and (F) efficacy vs. light dose (E_0), for various light intensity of 50, 100, 200 mW/cm^2, (for curves 1,2,3), without external oxygen source (*p*=0); *d*=33, k'=0.0001 (for type-II dominant) and for substrate [A]=50 uM.

Preprints (www.preprints.org) | NOT PEER-REVIEWED | Posted: 30 October 2018 doi:10.20944/preprints201805.0472.v2

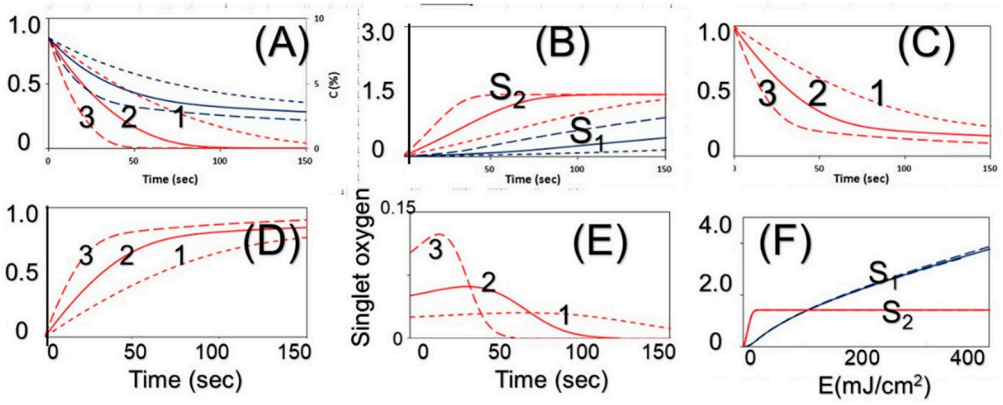

Fig. 5 Same as Fig. 4, but for a higher k'=0.05 and with external oxygen source (p=0.15), in which type-I and type-II coexist. Fig (B) and (F) show both S_1 (blue curves) and S_2 (red curves).

4. Conclusion

For the same dose, lower light intensity achieves a higher steady-state-efficacy (SSE) in type-I; in contrast to type-II, which has an equal SSE. Type-II process is also affected by the available oxygen. Higher light intensity produces more efficient singlet oxygen, resulting a higher transient efficacy, in which all intensities reach the same SSE when oxygen is completely depleted. With external oxygen, type-II efficacy increases with time, otherwise, it is governed only by the light dose, i.e., same dose achieves same efficacy. Moreover, type-II has an efficacy follows Bunsen Roscoe law (BRL), whereas type-I follows non-BRL. The photopolymerization dynamics may be defined by the availability of oxygen, where both type-I and –II coexist until the oxygen is depleted. The roles of light dose and PS concentration on the efficacy should be governed a new concept of a volume efficacy (Ve), first introduced by Lin [30], defined by the product of the crosslink (or gelation) depth (CD) and local [efficacy].

Acknowledgments: This work was supported by the internal grant of New Vision Inc. KT Chen is partially supported by the Ph. D program of Graduate Institute of Applied Science and Engineering, Fu Jen Catholic University, Taiwan.

Author Contributions: Conceptualization, Jui-Teng Lin; Data curation, Jui-Teng Lin and Da-Chuan Cheng; Formal analysis, Jui-Teng Lin; Funding acquisition, Hsia-Wei Liu and Da-Chuan Cheng; Methodology, Jui-Teng Lin; Project administration, Hsia-Wei Liu; Software, Kuo-Ti Chen and Da-Chuan Cheng; Supervision, Jui-Teng Lin.

Conflicts of Interest: Jui-Teng Lin is the CEO of New Vision Inc.

References

1. Fouassier J-P. Photoinitiation, Photo-polymerization, and Photocuring: Fundamentals and Applications. 1995, Hanser Gardner Publications Munich.
2. Anseth KS, Klok HA. Click chemistry in biomaterials, nanomedicine, and drug delivery. Biomacromolecules, 2016; 17:1–3.
3. Chen FM, Shi S. Principles of Tissue Engineering, 4th ed.; 2014, Elsevier: New York, NY, USA.
4. Drury JL, Mooney DJ. Hydrogels for tissue engineering: scaffold design variables and applications. Biomaterials 2003, 24, 4337–4351.
5. Pereira R, Bartolo P. Photopolymerizable hydrogels in regerative medicine and drug delivery. Top. Biomater. 2014, 6–28.
6. Chen MC, Garber L, Smoak M et al. In vitro and in vivo characterization of pentaerythritol triacrylate-co-trimethylolpropane nanocomposite scaffolds as potential bone augments and crafts. Tissu Eng. Part A 2015, 21, 320–331.
7. Chatani S, Gong T, Earle BA, Podgórski M, Bowman CN. Visible-light initiated thiol-Michael addition photopolymerization reactions. ACS Macro Lett. 2014; 3(4):315–318.
8. Mazaki T, Shiozaki Y, Yamane K, et al. A novel, visible light-induced, rapidly cross-linkable gelatin scaffold

for osteochondral tissue engineering Scientific Report, 2014, 4457, DOI: 10.1038/srep04457.

9. Zhang X, Xi W, Wang C, Podgórski M, Bowman CN. Visible-light-initiated thiol-Michael addition polymerizations with Coumarin-based photobase generators: another photoclick reaction strategy. ACS Macro Lett. 2016; 5:229–233.
10. Xi W, Peng H, Aguirre-Soto A, Kloxin CJ, Stansbury JW, Bowman CN. Spatial and temporal control of thiol-Michael addition via photocaged superbase in photopatterning and two-stage polymer network formation. Macromolecules. 2014; 47(18):6159–6165.
11. Shih H, Liu, HY, Lin CC. Improving gelation efficiency and cytocompatibility of visible light polymerized thiol-norbornene hydrogels via addition of soluble tyrosine. Biomater. Sci. 2017, 5:589–599.
12. Fairbanks BD, Schwartz MP, Bowman CN, Anseth KS. Photoinitiated polymerization of PEG-diacrylate with lithium phenyl-2,4,6-trimethylbenzoylphosphinate: Polymerization rate and cytocompatibility. Biomaterials. 2009, 30:6702–6707.
13. Zhu TC, Finlay JC, Zhou X, et al. Macroscopic modeling of the singlet oxygen production during PDT. Proc SPIE. 2007; 6427:6427O81–6427O812.
14. Kim MM, Ghogare AA, Greer A, Zhu TC et al. On the in vivo photochemical rate parameters for PDT reactive oxygen species modeling. Phys. Med. Biol. 2017, 62, R1–R48.
15. O'Brart NAL, O'Brart DPS, Aldahlawi et al, An Investigation of the effects of riboflavin concentration on the efficacy of corneal cross-Linking using an enzymatic resistance model in porcine corneas. Invest. Ophthalmol Vis Sci. 2018; 59: 1058-1065. doi:10.1167/iovs.17-22994.
16. Lin JT. Efficacy S-formula and kinetics of oxygen-mediated (type-II) and non-oxygen-mediated (type-I) corneal cross-linking. Ophthalmology Research. 2018; 8(1): 1-11.
17. Lin JT. A Critical Review on the Kinetics, Efficacy, Safety, Nonlinear Law and Optimal Protocols of Corneal Cross-linking. J Ophthalmology & Visual Neuroscinece, 2018; 3:017.
18. Terrones G, Pearlstein AJ. Effects of optical attenuation and consumption of a photobleaching initiator on local initiation rates in photopolymerizations. Macromolecules. 2001, 34: 3195–3204.
19. Kenning NS, Kriks D, El-Maazawi M, Scranton A. Spatial and temporal evolution of the photo initiation rate for thick polymer systems illuminated on both sides. Polym Int. 2005, 54: 1429–1439.
20. Miller GA, Gou L, Narayanan V, Scranton AB. Modeling of photobleaching for the photoinitiation of thick polymerization systems. J Polym Sci Part A Polym Chem 2002;40(6):793–808.
21. Okay O, Bowman CN. Kinetic modeling of thiol-ene reactions with both step and chain growth aspects. Macromol. Theory Simul. 2005; 14:267–277.
22. Reddy SK, Cramer NB, Kalvaitas M, Lee TY, Bowman CN. Mechanistic modelling and network properties of ternary thiol-vinyl photopolymerizations. Aust. J. Chem. 2006; 59(8):586–593.
23. Claudino M, Zhang X, Alim MD et al. Mechanistic kinetic modeling of Thiol–Michael addition photopolymerizations via photocaged "superbase" generators: An analytical approach. Macromolecules. 2016; 49(21): 8061–8074. doi:10.1021/acs.macromol.6b01605.
24. Lin JT, Liu HW. Cheng DC. Optimal focusing and scaling law for uniform photo-polymerization in a thick medium using a focused UV Laser. Polymers. 2014, 6:552-564. doi:10.3390/polym6020552.
25. Lin JT, Liu HW. Cheng DC. Modeling the kinetics of enhanced photo-polymerization under a collimated and a reflecting focused UV laser. Polymers. 2014, 6: 1489-1501.
26. Lin JT, KC Wang. Analytic formulas and numerical simulations for the dynamics of thick and non-uniform polymerization by a UV light. J Polym Res. 2016, 23: 53; DOI 10.1007/s10965-016-0934-4.
27. Lin JT. Optimal efficacy in light-activated biomedical systems and nonlinear laws versus linear Beer-Lambert law and Bunsen- Roscoe reciprocal law. Op Acc J Bio Eng & Biosc 1(5)- 2018. OAJBEA.MS.ID.000123.
28. Lin JT, Cheng DC. Modeling the efficacy profiles of UV-light activated corneal collagen crosslinking. PloS One. 2017;12:e0175002. DOI:10.1371/journal.pone.0175002.
29. Lin JT. A proposed concentration-controlled new protocol for optimal corneal crosslinking efficacy in the anterior stroma. Invest. Ophthalmol Vis Sci. 2018;59:431–432.
30. Lin JT. The role of stroma riboflavin concentration in the efficacy and depth of corneal crosslinking. Invest. Ophthalmol Vis Sci. 2018; 59:4449-4450.
31. Holmes R, Yang XB, Dunne et al, Thiol-Ene Photo-Click Collagen-PEG Hydrogels: Impact of Water-Soluble Photoinitiators on Cell Viability, Gelation Kinetics and Rheological Properties. Polymers 2017, 9, 226; doi:10.3390/polym9060226.

462 32. Zhu TC, Kim MM, Liang X et al. *In-vivo* singlet oxygen threshold doses for PDT. Photonics Lasers Med,
463 2015: 4:59-71.
464 33. Klimenko VV, Shmakov SV, Kaydanov et al. In vitro singlet oxygen threshold dose at PDT with
465 Radachlorin photosensitizer. 2017; SPIE Proc. Vol. 10417.
466 34. Lin JT. Advances of cancer synergic photo-therapy: kinetics and efficacy. Nov Appro in Can Study. 2018;
467 2(1). NACS.000529.2018. DOI: 10.31031/NACS.2018.02.000529.
468 35. Lin JT, Chen KT, Liu HW. Analysis the role of oxygen, light intensity, threshold dose and efficacy
469 improvement of anti-cancer via type-II photodynamic therapy. Nov Appro in Can Study. 2018; 2(1).
470 NACS.000533.2018. DOI: 10.31031/NACS.2018.02.000533.